TU Delft

Delft University of Technology

Document Version
Final published version

Licence
CC BY

Citation (APA)
Roberts, S., Raby, A., Boulton, S. J., Allsop, W., Antonini, A., van Balen, I., McGovern, D., Adams, K., Chandler, I., & More Authors (2025). Tsunami boulder transport in coastal environments: Insights from physical experiments and dimensional analysis. *Marine Geology*, *480*, Article 107474. https://doi.org/10.1016/j.margeo.2024.107474

Important note
To cite this publication, please use the final published version (if applicable).
Please check the document version above.

Copyright
In case the licence states “Dutch Copyright Act (Article 25fa)”, this publication was made available Green Open Access via the TU Delft Institutional Repository pursuant to Dutch Copyright Act (Article 25fa, the Taverne amendment). This provision does not affect copyright ownership.
Unless copyright is transferred by contract or statute, it remains with the copyright holder.

Sharing and reuse
Other than for strictly personal use, it is not permitted to download, forward or distribute the text or part of it, without the consent of the author(s) and/or copyright holder(s), unless the work is under an open content license such as Creative Commons.

Takedown policy
Please contact us and provide details if you believe this document breaches copyrights.
We will remove access to the work immediately and investigate your claim.

This work is downloaded from Delft University of Technology.

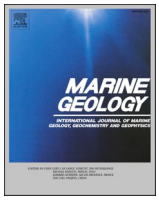
Marine Geology 480 (2025) 107474



Contents lists available at ScienceDirect

Marine Geology

journal homepage: www.elsevier.com/locate/margo



Research Article

Tsunami boulder transport in coastal environments: insights from physical experiments and dimensional analysis

Storm Roberts [a,*], Alison Raby [b], Sarah J. Boulton [a], William Allsop [c], Alessandro Antonini [d], Ivo van Balen [d], David McGovern [e], Keith Adams [e], Ian Chandler [f], Jonas Cels [g], Irene Manzella [a,h]

[a] School of Geography, Earth and Environmental Sciences, University of Plymouth, Drake's Circus, Plymouth PL4 8AA, UK
[b] School of Computing, Engineering and Maths, University of Plymouth, Drake's Circus, Plymouth PL4 8AA, UK
[c] William Allsop Consulting Ltd, The White House Denchworth Road, Grove, Wantage, Oxon, England OX12 0AR, UK
[d] Faculty of CEG, Delft University of Technology, Delft 2628, CN, Netherlands
[e] School of The Built Environment and Architecture, London South Bank University, London SE1 6LN, UK
[f] HR Wallingford, Howbery Park, Wallingford, Oxfordshire OX10 8BA, UK
[g] UCL EPICentre, Dept. Of Civil, Environmental and Geomatic Engineering, University College London, London WC1E 6BT, UK
[h] Centre for Disaster Resilience, University of Twente, Enshede, 7522, NH, Netherlands

ARTICLE INFO

Editor: Prof Edward Anthony

Keywords:
Tsunami
Physical experiment
Coastal boulder deposit
Dimensional analysis
Extreme waves

ABSTRACT

Coastal boulder deposits hold the potential to aid in the reconstruction of past extreme wave events. However, commonly used hydrodynamic equations for calculating wave heights from transported boulders can be inaccurate. New and alternative methods need to be explored in an interdisciplinary way to ensure a more complete picture of the phenomenon of boulder transport is achieved. Through the use of a physical experiment, this study aims to investigate the influence of different tsunami wave types, wave parameters and boulder shapes on boulder transport distance. The experimental results also allow for a novel application of dimensional analysis to enable comparisons with other experiments as well as a field case study. In the experiment an elongate irregularly shaped boulder showed transport distances up to 1 m farther than a cuboid shaped boulder under the influence of the same waves. The irregularly shaped boulder had a predominant transport mode of rolling, whereas the cuboid shaped boulder predominantly underwent sliding transport. Tsunami wave type also influenced boulder transport distances, with N-waves frequently showing greater transport than E-waves of a comparable wave steepness. Key offshore wave and boulder parameters were then compared through dimensional analysis using Buckingham's Pi Theorem, enabling comparisons to other datasets to be made. Data from another published experimental study and a field study in Settai, Japan, showed reasonable agreement, particularly for the shorter period field data. These findings emphasize the importance of incorporating boulder shape, wave type, and dimensional analysis into future studies, providing a foundation for more accurate reconstructions of past tsunami events.

1. Introduction

Tsunami and storm-transported coastal boulder deposits (CBDs) are found globally in a variety of coastal geomorphologic contexts, including as isolated boulders (Imamura et al., 2008), clusters and ridges (Cox et al., 2012) found on beaches (Goto et al., 2007; Lau et al., 2015), cliff tops (Williams and Hall, 2004; Cox et al., 2018), and even hundreds of metres inland on low lying topography (Nandasena et al., 2013). Although tsunami events in the past are generally studied using graded sediment sequences in the geological record (e.g., Dawson and Stewart, 2007), fine-grained deposits are not always present as they are prone to erosion. Larger clasts transported by extreme wave events are less likely to be eroded and swept away by recurring smaller events, particularly on rocky coastlines. As a result, CBDs offer an alternative, or additional way, to study the tsunami or storm record and even have the potential to be used as evidence towards the reconstruction of extreme wave events in the past (Nott, 1997, 2003).

One key technique for the reconstruction of these events is through the application of hydrodynamic equations to CBDs. Nott (1997, 2003) created the first iteration of hydrodynamic equations using inverse

* Corresponding author.
E-mail address: storm.roberts@plymouth.ac.uk (S. Roberts).

https://doi.org/10.1016/j.margeo.2024.107474
Received 17 August 2024; Received in revised form 18 December 2024; Accepted 31 December 2024
Available online 3 January 2025
0025-3227/© 2025 The Authors. Published by Elsevier B.V. This is an open access article under the CC BY license (http://creativecommons.org/licenses/by/4.0/).

modelling of boulder characteristics to make inferences about the causative wave parameters. The principle works by calculating the flow velocity necessary to initiate the motion of a boulder of a known size and density, from which the (tsunami or storm) wave height can then be estimated. Since these initial equations, the initiation-of-motion equations have been developed further (e.g., Pignatelli et al., 2009; Barbano et al., 2010; Benner et al., 2010; Nandasena et al., 2011) and have seen widespread use by geomorphologists (e.g., Costa et al., 2011; Shahhosseini et al., 2011; Engel and May, 2012; Boulton and Whitworth, 2018; Pepe et al., 2018). However, the limitations of these equations have been outlined for their uncertainty and potential misuse (Sugawara et al., 2014; Nandasena, 2020; Kennedy et al., 2021). For example, the values of coefficients (e.g., drag, lift), which the equations are sensitive to, are often varied between studies (Sugawara et al., 2014).

Recently, the initiation-of-motion equations have been further criticized in a systematic review by Cox et al. (2020) because of the inaccuracy in differentiating storm and tsunami events, as well as issues hindcasting their wave heights. A significant problem with the original Nott (2003) equation identified by Cox et al. (2020) is that it uses H_s to signify height of a storm wave at breaking point, which has often been conflated with the widely used term for significant wave height (also H_s). Significant wave height is the mean height measurement of the highest third of the waves recorded, usually by deep-water wave buoys. The wave height at breaking point which transported a boulder can be notably different to the significant wave height recorded offshore because shoaling processes affect wave heights on their coastal approach. Additionally, significant wave height is an average rather than a maximum value, so is smaller than any peak value at a location. Owing to the availability of offshore wave data from buoys and lack of wave data at the breaking point of waves, the ability to make connections between boulder transport and the offshore wave environment would be a more straightforward way to make comparisons between sites. Another limitation of the Nott (2003) hydrodynamic equations highlighted by Cox et al. (2020) is that the wave type parameter (δ) (which is the square of the Froude number (Fr) and is typically used to differentiate storm and tsunami wave heights) is assigned values of $Fr = 1$ for storm waves and $Fr = 2$ for tsunami waves. This choice of values is an oversimplification, as both tsunami and storm waves can exhibit a wide range of Froude values (Cox et al., 2020). As a result, the application of the Nott (2003) equations will always result in a storm wave exactly four times higher than a tsunami wave to move the same boulder. Consequently, Cox et al. (2020) recommend exploring new interdisciplinary approaches to overcome these problems, particularly through the increased use and integration of physical experiments and numerical modelling.

A range of physical experiments on CBD transport (Table 1) have been undertaken to start to constrain the influence of different tsunami wave parameters on boulder transport (Oetjen et al., 2021). The focus of these experiments has largely been to either; A) investigate the flow velocity required to initiate motion of a boulder (Bressan et al., 2018; Harry et al., 2019; Lodhi et al., 2020), or B) determine how different flow velocities influence boulder transport (Luccio et al., 1998; Petroff et al., 2001; Imamura et al., 2008; Nandasena and Tanaka, 2013; Liu et al., 2014; Oetjen et al., 2020; Watanabe et al., 2020). However, many experiments use a set-up featuring a dam break wave generation method in a dry or shallow water (< 5 cm) depth flume, only recording limited wave parameters like the flow velocity on the slope (e.g., Petroff et al., 2001; Nandasena and Tanaka, 2013; Lodhi et al., 2020) because this is the most straightforward set-up to investigate the influence of flow velocity on boulders. While only a limited number of experiments record wave parameters (Table 1) (e.g., wave height, wave period, flow depth, flow velocity) from offshore to onshore to give a complete picture of the entire event (e.g., Oetjen et al., 2020; Watanabe et al., 2020). It is important to record all the wave parameters, where possible, so that parameter relationships can be found throughout the wave process and comparisons between studies and real-world events can be made. A greater understanding of the influence of all the parameters involved is important for informing future models and alternative approaches to hindcasting waves with CBDs.

Kennedy et al. (2021) addressed the shortcomings of the initiation-of-motion equations, using dimensional analysis to differentiate between storm and tsunami-transported boulder deposits. Dimensional analysis facilitates the investigation of relationships between the fundamental quantities (mass, length, and time) of different physical characteristics relating to the problem studied. In the field of hydrodynamics, dimensional analysis is often used to create empirical equations between parameters when the physical processes are complex. Also, by removing dimensions, comparisons between different datasets are

Table 1
Previous experimental studies on tsunami boulder transport, where X_b is boulder transport distance, H is wave height, T is wave period, m is mass, ρ_s is boulder density, d is depth, and V is flow velocity on the slope.

Study	Parameter reported							Boulder shape	Beach slope	Wave generation method
	X_b (m)	H (m)	T (s)	m (kg)	ρ_s (kg/m^3)	d (m)	V (m/s)			
Luccio et al. (1998)	✓			~0.15— ~ 0.36	1500—2400	0	~1—2	Discoidal	3.5:100 slope followed by horizontal shore	Dam break
Petroff et al. (2001)	✓			0.0014—0.0376	2717	0.02	1.55	Cuboid	1:10 slope	Dam break
Imamura et al. (2008)	✓			0.007—0.033	1550—2710	0.012	1.5	Cuboid	1:10 slope	Dam break
Nandasena and Tanaka (2013)	✓			0.006—0.35	1985—2880	0	~0.7—1.3	Cuboid	1:20 slope	Dam break
Liu et al. (2014)	✓	✓		6.912	2400	0.1	~1.25—1.37	Cuboid	3.75:100 slope followed by horizontal shore	Dam break
Bressan et al. (2018)				0.053—0.15	1900—2600	0	~0.25	Cuboid	1:10 slope	Dam break
Harry et al. (2019)	✓			9.05E-7—8.18E-6	2600	0	8	Spherical	horizontal	Centrifuge
Lodhi et al. (2020)				0.07—0.19	2670	0.01	0.3—0.4	Cuboid	2:5 slope followed by flat bed	Dam break
Oetjen et al. (2020)	✓	✓	✓	1.43—1.49	2200	0.13—0.2	0.7	Cuboid, Irregular	Multiple shore types	Pump 'modified dam break'
Watanabe et al. (2020)	✓	✓	✓	0.35—0.53	2100—2500	4.5—0.9	2.6—3.6	Cuboid	1:100 slope	'wave maker'
This experiment	✓	✓	✓	0.077—0.082	2730	0.85—1.02	0.25—0.74	Cuboid, Irregular	1:30 slope	Tsunami Simulator

simplified, as limitations such as scale can be disregarded.

The upper parameter limits (elevation, distance inland, boulder size) of boulder deposition by storm waves were estimated by Kennedy et al. (2021) using dimensionless groups. Plotting dimensionless field parameters of boulder deposits with a known storm or tsunami emplacement mechanism allows for the upper limits of storm boulder transport to be constrained. The data below the upper limit is considered the storm envelope in which both storm and tsunami events could have emplaced the boulder. In contrast, dimensionless groups larger than this envelope were likely transported exclusively by tsunami events. Although Kennedy et al. (2021) identify new methods for differentiating storm and tsunami events, there is further potential for dimensional analysis to be used to integrate physical experiments into our understanding of CBD transport.

Therefore, this study aims to investigate the influence of boulder shape and tsunami wave parameters on boulder transport distance using dimensional analysis, so that better comparisons can be made between experiments as well as to field data. This aim will be achieved through the following objectives: 1) a physical experiment will be conducted to examine the influence of different wave and boulder parameters; 2) novel dimensional analysis will be used to explore the relationships between parameters and make comparisons with other studies, and 3) a case study of boulders transported by the 2011 tsunami in Settai, Japan will be used to test the application of dimensional analysis on real world deposits. Through this experimental investigation and application of dimensional analysis, this study will provide insights into boulder transport under the influence of tsunami waves, paving the way for future advancements in the hindcasting of tsunami waves with CBDs.

2. Methods

2.1. Experimental set-up

The experiments were conducted using the tsunami simulator at HR Wallingford, U.K., at a geometric scale of 1:50. A sketch of the experimental layout and instrument positions is given in Fig. 1. For each test the boulder models were placed with the same orientation on the 1:30 slope, along the still water line (SWL). Boulder transport distance (X_b) was recorded as the maximum distance up-slope caused by the first wave that produced motion; subsequent waves sometimes produced greater transport up-slope and drawdown sometimes caused down-slope motion. Transport distances were measured using a tape measure attached to the slope. Tests were repeated three times to ensure and determine the reproducibility of the results.

Two boulder shapes were selected for the experiments: a cuboid-shaped boulder model to provide comparisons to previous studies (e.g., Oetjen et al., 2020; Watanabe et al., 2020), and an irregular shaped boulder model to be more representative of real-world boulder deposits, in particular elongate, rounded boulders. Comparing results from the two boulder shapes provides insight into how well the findings from typical cuboid boulder model experiments can be applied to field studies with non-cuboid boulders. The cuboid boulder model had dimensions of 2.7 × 3.3 × 3.4 cm (± 0.01 cm), a volume of 30.3 cm^3, and a dry weight of 82 g (Fig. 2). The irregular boulder model had approximate dimensions of 7.5 × 3 × 2.3 cm, an approximate volume of 28.5 cm^3, and a dry weight of 77 g. Both boulder models were made of the same limestone, which had a density of 2700 kg/m^3. Density (ρ_s) was calculated from volume measurements recorded using the water displacement method and mass (m) was determined using a laboratory balance.

Flow velocity (V) on the slope was measured using an acoustic doppler velocimeter (ADV) (Nortek Vectrino), placed in line with the boulder starting position (d = 0 m). It was defined as the maximum velocity from a moving average of the signal for the wave under consideration, using 25 data points (the data acquisition frequency of the ADV being 25 Hz). One wave gauge (WG1) recorded offshore wave information between the tsunami simulator and the toe of the slope, and a second wave gauge (WG2) recorded data part way up the slope (Fig. 1), corresponding to the SWL for the d = 1.02 m tests. Three wave types were examined: N-waves, which are trough led waves (Fig. 3a), E-waves, which are crest led waves (Fig. 3b), and bore waves, which are broken, crest-led waves with a steep front (Fig. 3c). The WG1 data allows for the determination of wave period (T) and wave height (H) for each wave. The wave height of N-waves is determined from the trough level to the following crest, whereas the E-waves and bore heights are determined from the crest to the following trough (Fig. 3). Water depth (d) was recorded in line with WG1. Similarly, wave period and wave height were determined using surface elevation measurements from WG1 as it is beyond the sloping bathymetry and thus interference from reflections from the underwater beach slope is reduced. WG1 is also far enough from the tsunami generator for the waves to be fully developed. Water depth was kept constant at 1.02 m for all tests except for three of the bore wave tests, which used a lower water depth of 0.85 m to additionally investigate the effects of changing flow depth on these waves. Flow depth on the slope was determined using WG2 and recorded as the maximum flow depth reached during each test. Gravitational acceleration (g) is assumed to be 9.81 m/s^2. The slope was made of plywood, which when wetted had a measured static friction of between 0.5 and 0.6 using a Newton meter.

The tsunami simulator uses a pneumatic long-wave generator to create repeatable waves with significantly longer wavelengths than other methods (McGovern et al., 2018), such as dam break wave generation, commonly used in tsunami boulder physical experiments (i.e., Oetjen et al., 2021). Therefore, by using the tsunami simulator, offshore waveforms with more realistic parameters than generated in standard flumes can be achieved.

2.2. Dimensional analysis

Buckingham's Pi Theorem was used to conduct dimensional analysis in a systematic way (Buckingham, 1915; Hughes, 1993). The theorem provides a method for forming a complete set of dimensionless parameters from a given set of variables (Hughes, 1993). The theorem states that if there are "n" variables in a dimensionally homogenous equation, the number of dimensionless products to form a complete set is equal to "n-r" where "r" is the number of primary dimensions (for example mass, length, time) found in the variables. The dimensionless products that make this complete set are referred to as Π (Pi) groups. The completed equation can be written as

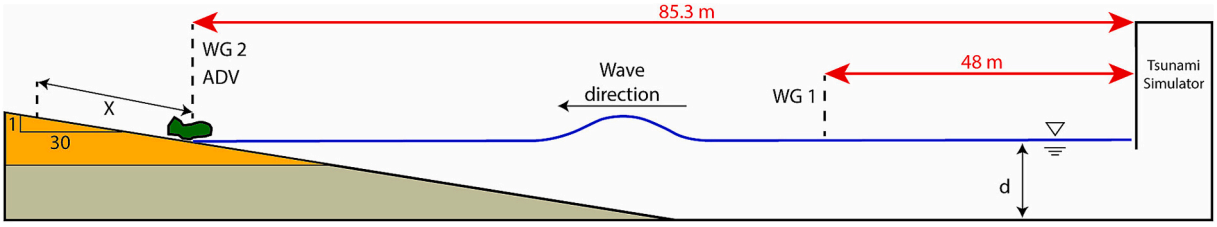


Fig. 1. Experimental setup, where X is the maximum distance the boulder (X_b) and the wave (X_w) travelled along the slope, d = water depth, WG = wave gauge, and ADV = acoustic doppler velocimeter. The yellow slope area is constructed from marine plywood, whilst the grey slope and rest of the flume is concrete.

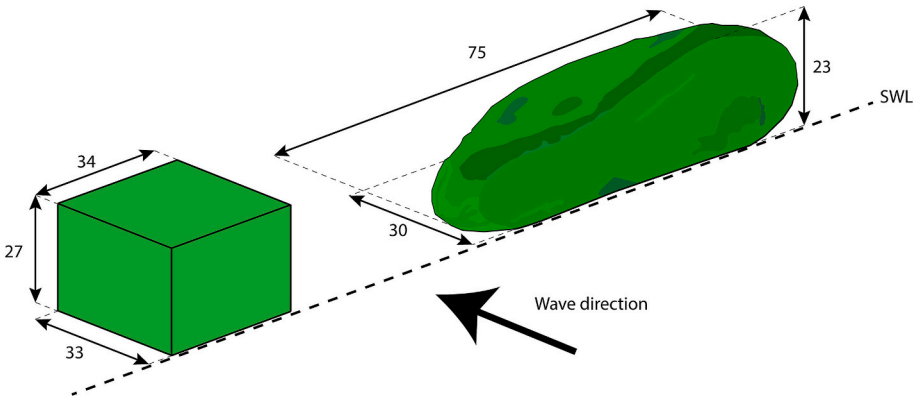


Fig. 2. Sketch showing model boulder dimensions (mm) and position on still water line (SWL).

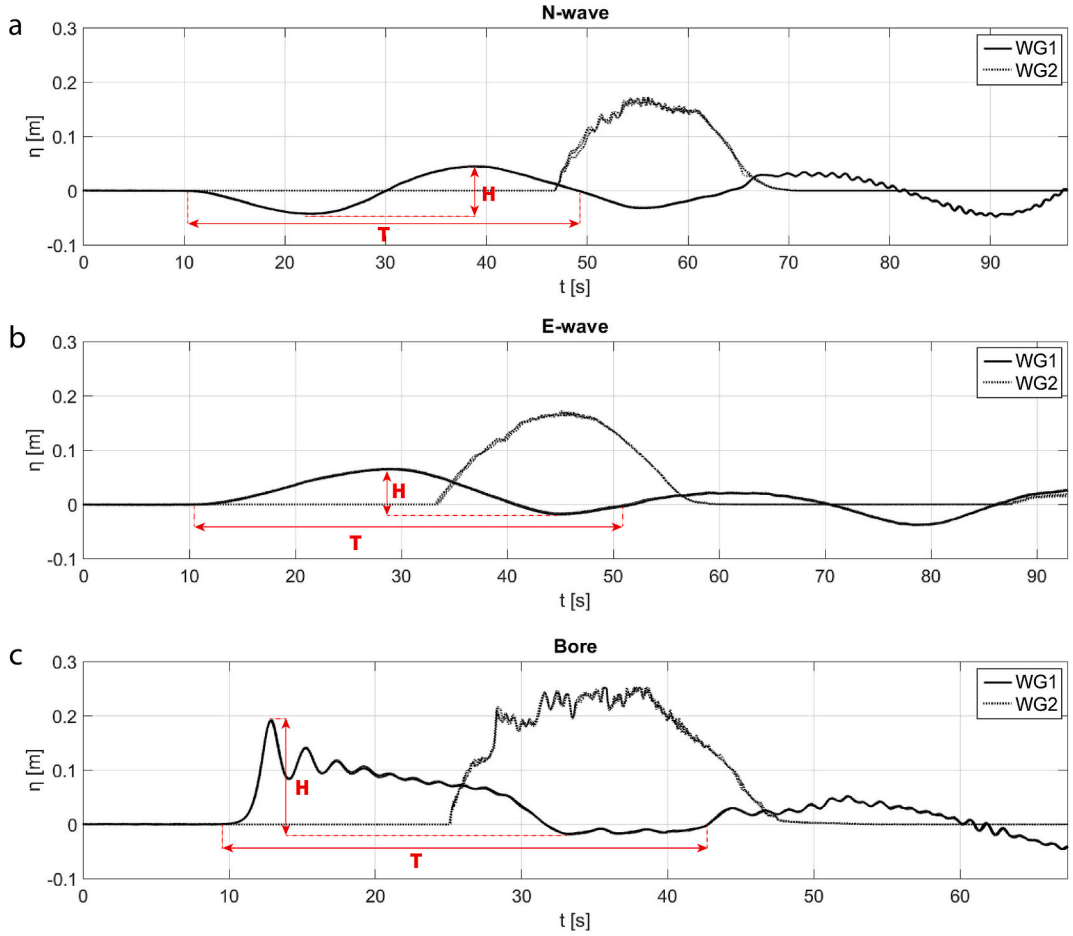


Fig. 3. Wave gauge data of three overlaid runs for N-waves (test # 7), E-waves (test # 2), and Bore-waves (test # 16), with H and T definitions for each wave type.

Table 2
Selected parameters and their associated dimensions where X_b is boulder transport distance, H is wave height, m is boulder mass, ρ_s is boulder density, T is wave period, d is water depth, g is gravity, u is water particle velocity, and D_n is nominal boulder diameter.

	X_b (m)	H (m)	m (kg)	ρ_s (kg/m^3)	T (s)	d (m)	g (m/s^2)	u (m/s)	D_n (m)
Mass	0	0	1	1	0	0	0	0	0
Length	1	1	0	- 3	0	1	1	1	1
Time	0	0	0	0	1	0	- 2	- 1	0

$$\Pi_1 = f(\Pi_2, \Pi_3, \ldots, \Pi_{n-r}) \quad (1)$$

where the numbered Π groups are related by some function f.

Only the variables most significant to the problem were selected (Table 2). To make connections with typical wave characteristics, wave height (H), wave period (T), water depth (d), gravity (g), and water particle velocity (u) were selected. Water particle velocity (u) is distinct from the bulk flow velocity on the slope (V); only the water particle velocity is used in the dimensional analysis. To represent the boulder, mass (m), density (ρ_s), nominal boulder diameter (D_n), and the transport distance (X_b) were chosen. The influence of other parameters (e.g., slope angle, friction) were considered but not included because they were not varied in the experiment so were not tested in this study.

Through the use of Buckingham's Pi Theorem, the following six Π groups were created:

$$\Pi_1 = \frac{d}{H} \quad (2)$$

$$\Pi_2 = \frac{uT}{H} \quad (3)$$

$$\Pi_3 = \frac{gT^2}{H} \quad (4)$$

$$\Pi_4 = \frac{D_n}{H} \quad (5)$$

$$\Pi_5 = \frac{m}{H^3\rho_s} = \frac{{D_n}^3}{H^3} \quad (6)$$

$$\Pi_6 = \frac{X_b}{H} = f_1\left(\frac{d}{H}, \frac{uT}{H}, \frac{gT^2}{H}, \frac{m}{H^3\rho_s}, \frac{{D_n}^3}{H^3}\right) \quad (7)$$

where boulder nominal diameter $D_n = \sqrt[3]{m/\rho_s}$, water particle velocity $u = c(\eta/d)$ (Svendsen, 2006), shallow water wave celerity $c = \sqrt{gd}$ and where η is the wave crest elevation measured with respect to the still water level. Actually, the celerity of a bore wave generated in this way has a maximum value of $2\sqrt{gd}$ though this decays rapidly in space and time to a value of about $\sqrt{gd}$ (Yang et al., 2022), so the latter expression is used here.

A limitation of this approach is that every additional Π group increases the complexity and makes the determination of an empirical formulation more difficult (Munson et al., 2014). When more than six variables are selected, with more than three associated pi groups, the pi groups cannot all be plotted on a single graph making it difficult to determine the form of empirical relationships between groups. Therefore, Principal Component Analysis (PCA) is applied to the standardized (i.e. centered to have mean 0 and scaled to have standard deviation 1) dimensionless groups to determine which are most influential in describing the problem. PCA is a statistical technique that reduces dataset dimensionality by transforming the data into principal components which capture the most variance in the data, while the standardisation procedure is required to ensure an equal weighting of the variables in the dataset. This procedure results in the first three principal components capturing 96.6 % of the variance in the data (Supp. Figs. 1; 2). Within these three principal components, the dimensionless groups in Π_2, Π_5, and Π_6 are selected for visualizing the dimensional analysis, as they have the greatest loadings (Supp. Fig. 1) and explain the variability in different ways (Supp. Fig. 3). With the three Pi groups defined, the measured data can be plotted on a dimensionless graph to determine the nature of the relationship between the parameters. Furthermore, experiments or field measurements at different geometric scales can be compared to experimental data.

2.3. Settai case study

To test the application of the dimensional analysis approach to field data, a case study example is necessary. The 2011 Tōhoku tsunami caused the movement of boulders and other debris throughout the impacted coastline of northeast Honshu, Japan (Nandasena et al., 2013; Iwai and Goto, 2021). In Settai, Iwate prefecture, several boulders were plucked and transported from rock faces surrounding the beach and river mouth, then transported hundreds of metres inland by the tsunami (Fig. 4a; b; c). The topography of the Settai River valley (Fig. 4d) is relatively flat and gently sloping (approx. 1:100) making it geomorphologically comparable to flume tank experiments on simple shore profiles. The location, combined with field data collected by Nandasena et al. (2013) and the availability of local offshore tsunami wave data (Shimozono et al., 2014), make Settai a suitable case study to compare to the experimental data.

The wave parameters H and T were determined from a nearby GPS buoy GB804 (d = 200 m) as shown in Figs. 4a; e (Shimozono et al., 2014). The 2011 Tōhoku tsunami wave parameters were determined in two ways: as a long period wave (orange line in Fig. 4e), and as a short period wave (purple line in Fig. 4e), to investigate the influence of the wave parameter definition. The two step waveform of the 2011 Tōhoku tsunami can be explained by slip on the deep fault contributing to the long period of the tsunami, alongside a delayed large shallow slip near the trench axis causing the shorter period but high wave height crest (Satake et al., 2013). The deep slip contributes to the significant horizontal inundation (Satake et al., 2013), but the shallow slip is responsible for the larger wave heights, impulsivity, and run-up seen along the Sanriku Coast (Yamazaki et al., 2018). Transported boulder data, including mass, density, and transport distance measurements, were taken from Nandasena et al. (2013), with transport distances confirmed using post-tsunami Landsat (2011) imagery.

3. Results

3.1. Experiment results

A total of 51 tests were conducted on each of the two boulder shapes, 12 of which used E-waves, 33 N-waves and 6 bore waves. All the tests conducted are summarized in the supporting information (S. Table 1). The waves generated by the tsunami simulator were highly reproducible (Fig. 3), with wave periods within 2 % (except for tests # 1iii, 10iii, 16i) of the mean, and wave heights within 2 % (except for tests # 1i, 7) of the mean, over three runs. Boulder transport distances were fairly consistent, with boulders transported within tens of centimetres of each other, although there was a greater range in boulder transport distance than there was for wave parameter variability. The bore waves showed the greatest range in transport distances for identical waves. For example, in the 1.02 m water depth tests (# 16i, 16ii, 16iii) the irregular boulder moved between 4.81 and 6.38 m. The $T = \sim$30 s N-wave tests (# 6i, 6ii, 6iii) also showed a wide range of transport distances with the irregular boulder transport distance ranging from 0.87 to 2.28 m. Typically, the irregular boulder had a slightly wider range of transport distances than the cuboid boulder over three tests, with the largest transport difference recorded (1 m) during the $T = \sim$22 s N-wave tests (# 5i, 5ii,5iii). Owing to the consistency of the wave generation, and the care taken with boulder placement between tests, any differences in transport distance over the three runs were likely caused by turbulence associated with wave breaking. To investigate the effects of boulder shape and wave type on boulder transport distance, boulder transport distance is firstly compared against a variety of wave parameters (Fig. 5).

Tests began with long wave periods (240 s), none of which produced movement. Wave periods were then gradually reduced to identify where boulder transport would be initiated. Wave periods examined ranged from 240 to 20 s for N-waves and 85–36 s for E-waves (Fig. 5a). The longest wave period that caused boulder movement was during a $T = 58$

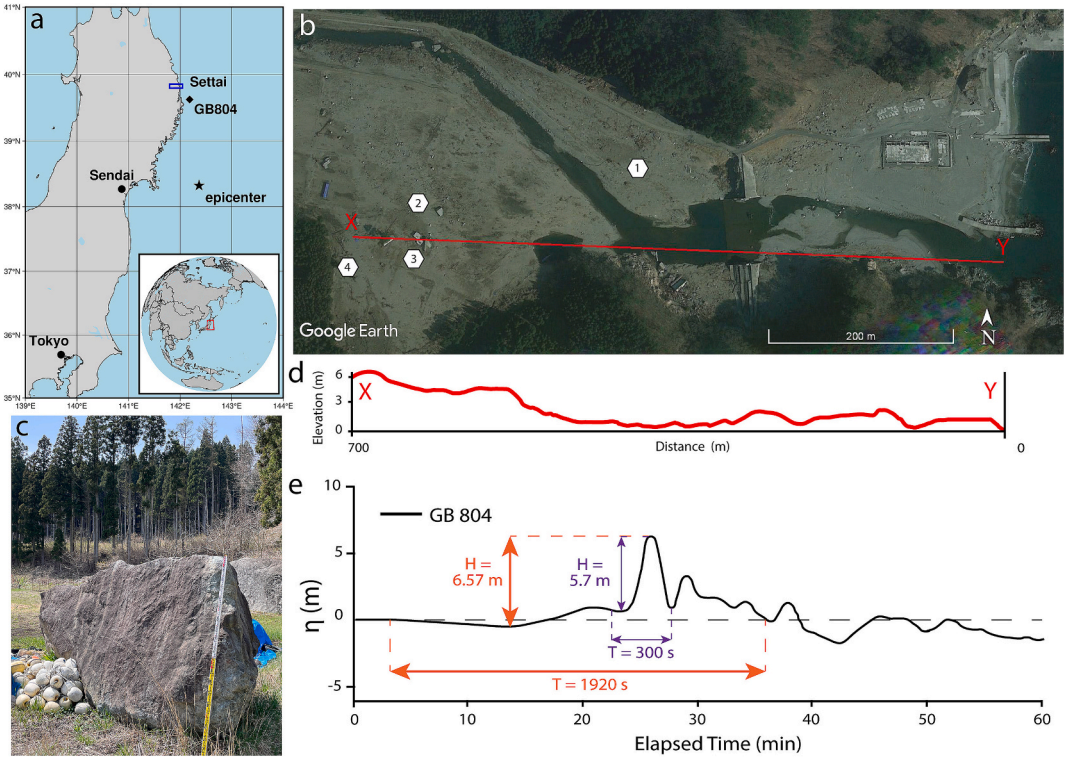


Fig. 4. Case study example of a coastal boulders transported by the 2011 Tōhoku tsunami in Settai, Japan: a) map of north Honshu, Japan featuring the location of the Settai site, GPS buoy 804 and epicenter of the 2011 earthquake; b) boulder locations in the aftermath of the tsunami April 5, 2011 (Landsat, 2011); c) field photo example of boulder #4; d) Topographic profile, and e) The waveform from the 2011 tsunami recorded at GB 804 modified from Shimozono et al. (2014).

s; $H = 0.06$ m N-wave test that caused the irregular boulder to be moved by 0.005 m. The shorter wave periods resulted in the greatest transport distances. However, it is important to note that for this investigation, the generated wave heights are typically lower for the long period waves due to generation mechanism limitations, i.e. the simulator has an upper limit to the volume of water that can be released.

Measured wave height at WG1 ranged from ~0.05 m to ~0.225 m, with the E- and N-waves having a maximum wave height of 0.097 m (Fig. 5b). Generally, as wave height increases so does boulder transport distance, but irregular boulders (circles; Fig. 5) generally move farther than cuboid boulders (squares; Fig. 5) for the same wave height. When wave height becomes large enough for boulders to begin moving, transport distance rapidly increases for the E-waves ($H > 0.08$ m); whereas for N-waves there is a steadier increase ($H = 0.06$–0.08 m) before a rapid increase in displacement ($H > 0.08$ m). At larger wave height values of the bore waves ($H = 0.2$–0.24 m) transport distance appears to be less sensitive to increases in wave height.

Wave steepness (H/L where wavelength $L = CT$) accounts for both the height and length of the waves. All three wave types show a similar trend, with boulder transport distance increasing as the wave steepness increases (Fig. 5c). However, the irregular boulder is generally transported farther than the cuboid at a similar wave steepness for the E- and N-waves, and comparable transport distances for the steeper bore waves. The wave steepness is also used in determining the breaking wave type using the Iribarren number $\xi = tan\alpha/\sqrt{H/L}$ where α is the slope angle (Fig. 5d). Boulder transport distance shows a moderate trend when plotted against the Iribarren number, with larger transport distances corresponding to lower Iribarren number values. This trend does not necessarily indicate that the type of wave breaking (e.g., spilling, plunging, surging) causing differences in boulder transport distance, because the smaller Iribarren number values are also associated with the largest wave heights.

The six bore wave runs additionally aimed to assess the effect of the water depth on boulder transport so that the wave characteristics were kept constant and only the water depth was varied between 1.02 and 0.85 m (Fig. 5c). The lower water depth resulted in a greater wave height (Fig. 5b), but wave period remained the same (Fig. 5a). The boulder models were placed at the new lower SWL for the three runs at 0.85 m water depth. As a result, there is no plotted slope flow velocity data (Fig. 5e) or flow depth (Fig. 5f) for the lower water depth run because the ADV and WG2 could not be moved down the slope owing to a shared flume arrangement.

Flow velocity shows a positive correlation with maximum transport distances (Fig. 5e). The lowest velocity to move a boulder was 0.27 m/s achieving just 0.005 m of movement, whereas the fastest recorded velocity of 0.71 m/s moved the irregular boulder the furthest recorded distance of 6.38 m. There is a range of transport distances below the maximum velocity values, which is in part caused by boulder shape (Fig. 5e). As flow velocity increases, so does the transport distance. However, irregular boulders exhibit a greater rate of increase in transport distance with flow velocity compared to cuboid boulders. At higher flow velocity values generated by the bore waves, the range of transport distance is smaller for the two boulder types, for similarly sized waves.

Maximum flow depth ranged from 0.015 to 0.2 m (Fig. 5f). The smallest maximum flow depth recorded during the tests generating boulder movement was 0.122 m, produced by an N-wave ($H = 0.097$ m; $T = 22.4$ s). Longer period waves could produce deeper maximum flow depths but they did not move the boulder models. For example, the largest comparable N-wave flow depth that did not result in movement of the cuboid boulder was 0.167 m with parameters $H = 0.067$ and $T = 45$ s.

The mode of transport for each boulder in each test is important to consider because it is thought to have an influence on transport distance (Imamura et al., 2008). The cuboid boulder model was predominantly transported by sliding, sometimes after being overturned by the initial wave impact (Supp. Table 1). The cuboid boulder was only transported predominantly by rolling during one bore wave test (# 17ii).

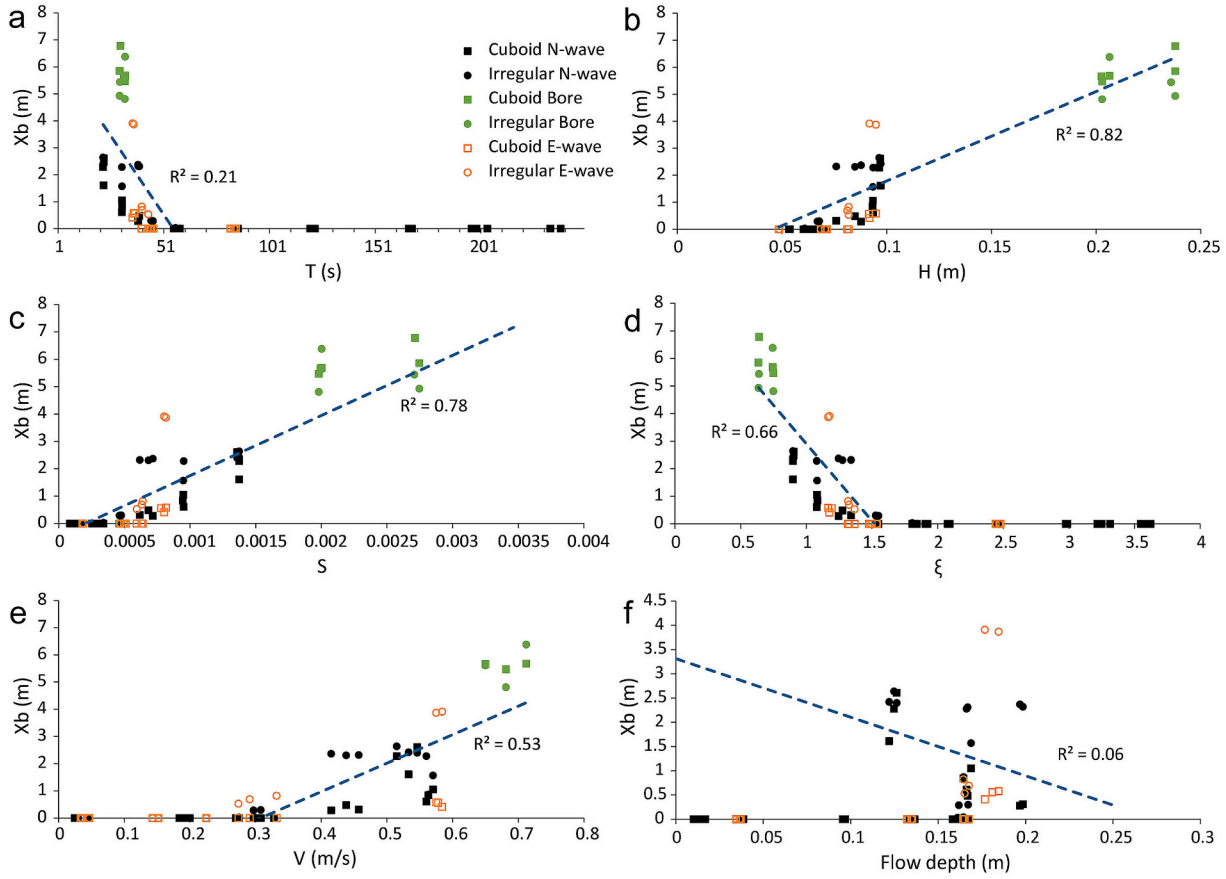


Fig. 5. Boulder transport distance (X_b) plotted against a) wave period (T), b) wave height (H), c) wave steepness (S), d) Iribarren number (ξ), e) flow velocity (V) at the SWL, and f) flow depth at the SWL. Trendlines for moved boulders only are shown in blue.

Conversely, the irregular boulder was transported via rolling in most cases, but did also undergo predominantly sliding transport in several tests (e.g., tests # 10 & 7). When sliding, the irregular boulder was transported with its long axis perpendicular to the flow and observed to shuffle, with the left and right side moving slightly ahead in turn. Both the cuboid and irregular boulder were observed to slide to a stop at the end of their rolling transport, with the irregular boulder shape occasionally rolling once forwards or back to reach a stable position at the end of transport.

Additionally, the boulder transport distance up the slope is plotted against the maximum distance the wave travelled along the slope in the absence of boulders (X_w) (Fig. 6). Distance X_w should not be confused with run-up or inundation, which are the vertical and horizontal measures of maximum wave motion respectively. Only the N- and E-waves have X_w data because the bore waves travelled beyond the end of the slope and could therefore not be measured. The maximum boulder transport distance shows a positive trend against X_w, with the furthest transport distance occurring at the furthest wave travel distance. Similar to flow velocity, there is a wide range of transport distances below the maximum values for similar wave distances. The smallest X_w to move a boulder was a 4.6 m N-wave, but an E-wave with a transport distance of 4.7 m did not move the boulder. The E-wave in this case had a flow velocity 0.1 m/s slower than that of the N-wave, despite having a similar wave steepness (Supp. Table 1). As might be expected, X_w always considerably exceeds X_b and at larger X_w values X_b becomes more variable.

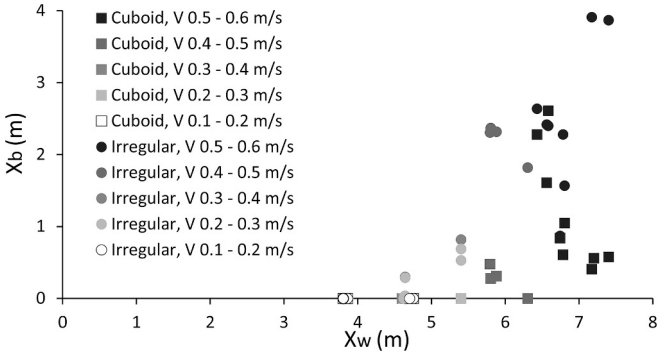


Fig. 6. Boulder transport distance (X_b) versus maximum water travel distance (X_w) symbolised by flow velocity and boulder shape.

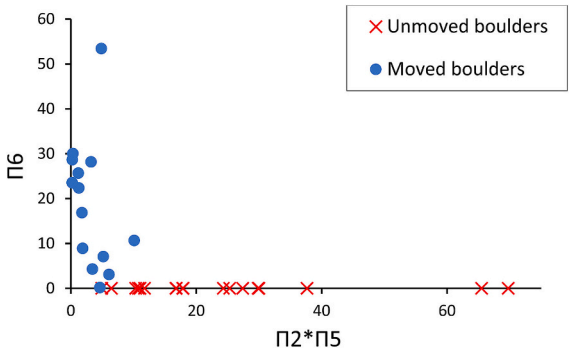


Fig. 7. A graphical representation of the relationship between Π_6 and Π_2*Π_5 for the transported (circles) and unmoved (crosses) boulders.

3.2. Dimensional analysis results

To understand the interdependencies of all the parameters, and to make comparisons with other datasets, the experimental data can be substituted into the defined dimensionless Π groups (Fig. 7). The upper limits of Π_6 (X_b/H) and $\Pi_2{*}\Pi_5$ ($(uT/H){*}\left(D_n{}^3/H^3\right)$) for the transported boulders are important because these potentially represent a window in which tsunami boulders are most likely to be transported within. Test # 1, an irregular boulder E-wave test with the greatest wave height and shortest wave period, shows a much greater Π_6 value than the rest of the tests. The largest $\Pi_2{*}\Pi_5$ value to transport a boulder was 10.67 representing the limit for transport occurring in the experiment.

3.3. Settai results

Boulder measurements were taken from Nandasena et al. (2013) and compared to the experimental data (Table 3). The selected boulders varied in size from 4.3 m^3 to 11.4 m^3, with boulder # 2 being most similar to the 1:50 scaled version of the experiment (Table 3). Interestingly, the heaviest boulder, Settai Boulder # 4 (Fig. 4), saw the greatest travel distance of 520 m. In terms of shape, Settai Boulders # 1–4 are subangular to angular (Nandasena et al., 2013) with a low sphericity. The Settai boulders are more similar in shape to the irregular boulder in the experiment, with a similarly elongate form, although more angular than the boulder model.

The two sets of wave parameters used for the Settai case study are compared to the most similar waves tested during the experiment (Table 4). The "depth adjusted" wave heights were transformed from 200 m depth to 51 m depth (scaling up the 1.02 m lab water depth) to be a more representative comparison, but the unmodified data was not used in any equations after this point. To adjust the wave height for different depths the conservation of energy flux equation was used, $H_0^2\sqrt{gd_0} = H_1^2\sqrt{gd_1}$, where the subscript '0' represents the offshore and '1' represents onshore parameters (Svendsen, 2006). The tsunami simulator generated waves with a similar height and a similar period to the depth-adjusted Settai long period (SLP) wave, but not simultaneously as the simulator could not maintain large wave heights for such extended periods. The depth-adjusted Settai short period (SSP) was most similar to the bore waves generated in the experiment in terms of both height and period simultaneously.

4. Discussion

4.1. Parameter influence in the experiment

The ultimate aim of CBD research is to be able to hindcast extreme wave events using boulders to identify flood-prone areas. To achieve this aim, connections must be made between parameters that can be measured/determined in the field and that can then be tested in laboratory experiments. The offshore (wave height and period) and onshore (flow velocity) wave parameters are some of the information that researchers (e.g., Nott, 2003; Kennedy et al., 2021) aim to determine from the available field parameters (boulder size, shape, density, weight, elevation, distance from source, run-up, transport mode, bottom roughness and flow depth).

Table 3
Boulder parameter comparison between the Settai case study and experiment.

	Vol (m^3)	*m* (kg)	ρ_s (kg/m^3)	X_b (m)
Irregular boulder scaled up (this study)	3.5	9450	2700	0–339
Cuboid boulder scaled up (this study)	3.8	10,224	2700	0–319
Settai Boulder # 1	8.3	20,388	2460	230
Settai Boulder # 2	4.3	10,924	2550	430
Settai Boulder # 3	6.5	15,587	2410	440
Settai Boulder # 4	11.4	30,045	2630	520

Table 4
Wave size comparisons between 2011 tsunami and different laboratory generated waves, at full-scale.

	Test #	Wave type	*d* (m)	*H* (m)	*T* (s)
Settai long period (SLP)	–	–	200	6.57	1920
Settai short period (SSP)	–	–	200	5.7	300
SLP depth adjusted	–	–	51	9.3	1920
SSP depth adjusted	–	–	51	8	300
Experiment: closest to SLP *H*	16iii	bore	51	10.1	226
Experiment: closest to SLP *T*	15iii	N-wave	51	3	1689
Experiment: largest *H* recorded	17ii	bore	42.5	11.9	212
Experiment: longest *T* & smallest *H* to move a boulder	10iii	N-wave	51	3	414

4.1.1. Wave parameters

One parameter that has seen significant amount of research in boulder transport experiments is the flow velocity at the boulder location (Nandasena and Tanaka, 2013; Bressan et al., 2018) because flow velocity has a significant role in the initiation of boulder motion. This relationship is demonstrated by the trend between flow velocity and transport distance (Fig. 5e). Furthermore, flow velocity forms the basis for the hydrodynamic equations that aim to calculate when motion will be initiated for a boulder (Nott, 2003). Owing to the critique of the initiation-of-motion approach, we instead use the experiment to investigate the relationship between offshore wave parameters and boulder transport, flow velocity and flow depth to build upon alternative methods for comparing physical experiments and field data.

The effects of the offshore wave parameters (*H*, *T*) cannot be examined in isolation because neither was held constant whilst the other was varied. Owing to the constraint of the generator's maximum water volume, wave period generally decreased as a function of increasing wave height. A contrast in wave period is the most distinctive difference between storm and tsunami waves (Open University, 1999), so it is logical to include the parameter when attempting to make hydrodynamic equations that can differentiate them. As the experiment has shown, both wave height and wave period are key parameters when describing the offshore environment, and wave steepness is a good way of combining both (Fig. 5c).

As waves become steeper boulder transport distance increases, but this occurs at different rates for different wave types (Fig. 5c). Generally, at similar wave steepness values (< 0.001), N-waves transport the boulder farther than E-waves. However, the irregular boulders transported by the steepest E-waves show the greatest transport distances of any E- or N-wave. Additional, E-wave boulder transport data for steeper waves would help discern if this indicates E-waves have greater transport distances than N-waves when impacted by steeper waves (> 0.001). Previous studies have not considered the difference in influence of N- and E-waves on boulder transport, as their primary focus has been on measuring flow velocity on the slope rather than identifying offshore wave parameters (Table 1).

The steepness of a wave, combined with the slope, determines the Iribarren number (ξ), which defines the wave breaking characteristics. Owing to the slope remaining constant, the Iribarren number is only influenced by the steepness of the wave in this study. This experiment resulted in a wide range of Iribarren numbers (0.57–3.62), with boulders only moving at values <1.85. The bore waves are plunging waves, $\xi < 0.65$, close to becoming spilling waves (< 0.5), with the largest transport distances. Whereas, for the E- and N-waves $\xi > 0.9$, making them plunging waves, with the exception of four of the longest period waves that were surging (Supp. Table 1). However, these four waves did not result in boulder movement. The Iribarren number influence suffers from the same issue of wave steepness influence in that it was not

possible to consider underlying parameters (H, T) in isolation.

The maximum distance water travels inland (X_w) is often recorded in the field by inundation and run-up measurements, either immediately after a tsunami event by the high-water mark or recorded in the sedimentological record as the furthest distances inland tsunami deposits can be located (e.g., Chagué-Goff et al., 2015; Iwai and Goto, 2021). In the experiment (Fig. 6), boulder transport distance (X_b) and maximum distance the wave travelled up the slope (X_w) showed that maximum X_b values have a trend as a function of X_w but the data has a wide range of values below the maxima. Therefore, although X_w can be recorded in the field, it is not a strong indicator of expected X_b, as X_b varies significantly at different $X_w$values. However, X_w could offer some indication of maximum boulder transport distances, with the caveat that there is significant variation.

4.1.2. Boulder parameters

The experiment used two boulders with a similar volume and mass, but different shapes, to highlight how the shape of the boulder model influences transport distance. The irregular boulder was observed to move through overturning and rolling; in comparison to the cuboid boulder which was largely transported via sliding with occasional overturning. The rounded, more elongate shape of the irregular boulder lends itself to rolling transport more than the cuboid boulder. Rolling transport is thought to lead to greater transport distances than sliding transport because of factors such as the reduced effects of bottom friction, but further research is required (Oetjen et al., 2020). Field research on CBDs often does not consider the shape of the boulders recorded, instead opting just to measure the boulders size/weight, despite the influence shape may have on where a boulder is deposited. Descriptions of field boulders shape will become more important in future as the influence of different boulder shapes is better quantified.

At different flow velocities at the boulder location the influence of shape is evident (Fig. 5e), owing in part to different modes of transport. The irregular boulder shows a positive linear correlation between transport distance and velocity, whilst the cuboid boulder shows a gradual increase in transport distance followed by a large increase in transport distance between 0.5 and 0.6 m/s (Fig. 5e). The increase in transport distance of the cuboid boulder may be caused by the change from entirely sliding to more overturning/rolling transport (Nandasena et al., 2022).

Both the irregular and cuboid boulders have similar transport distances when impacted by the high velocity bore waves. This could be because at very high flow velocities the boulder models underwent more rolling/saltation transportation, so the influence of shape was reduced and instead their similar mass resulted in a similar transport distance (Fig. 5e). The irregular boulder undergoes initial transport at velocities as low as 0.27 m/s, compared to 0.42 m/s for the cuboid boulder, possibly owing to its irregular shape allowing for more lift under the boulder and less bottom friction. Conversely, the cuboid boulder has a flat base, parallel to the slope, preventing the ingress of water under it to generate lift.

A wider range of boulder shapes need to be tested to further investigate factors that increase or decrease boulder transport distance. Furthermore, a way of quantifying shape within hydrodynamic equations needs to be developed beyond the three main boulder dimensions; roundness and sphericity must also be considered. For example, although in this study the elongate rounded irregular boulder was transported farther than the cuboid boulder control, in other studies such Oetjen et al. (2020) a regular cuboid had an average transport distance 47 % greater than that of a more rounded realistic boulder. These differences in transport distance could be caused by differences in slope, friction, or the difference in sphericity of the boulders (Nandasena et al., 2022). Additional investigation of shape is necessary to comprehensively explain these differences.

In this study, boulders were placed in a subaerial position just above the SWL with a long axis perpendicular to flow. By contrast other studies (e.g., Nandasena and Tanaka, 2013; Oetjen et al., 2020) explore different starting positions (subaerial, partially submerged, submerged) and boulder orientations relative to flow. Oetjen et al. (2020) show that the influence of starting position (partially submerged to subaerial) caused a difference in transport distance of 360 % for a flat cuboid shaped boulder. This observation suggests that minor differences in boulder starting position have a significant effect on the transport distance, which should be considered when making comparisons between experimental and field data. Moreover, the limited number of physical boulder experiments (Table 1) hinders comparisons especially as these are conducted at different scales, with different shore set ups, wave generation methods, and different boulder models. To facilitate comparisons and reduce the effects of some of these differences, dimensional analysis can be used to compare the relationships between parameters (wave and boulder) between different studies and the field.

4.2. Dimensional analysis

To investigate the relationships between offshore wave parameters and boulder transport, as well as to compare experimental studies and field sites, dimensional analysis can be used. Previously, dimensional analysis has been used by Kennedy et al. (2021) to make connections between offshore storm wave heights and boulder deposition location (elevation/distance inland) to better differentiate storm and tsunami boulder deposits. The current study expands this approach to consider additional wave information to devise new techniques for the comparison of physical tsunami experiments and field events.

The three selected dimensionless groups represent dimensionless boulder transport ($\Pi_6 = X_b/H$), dimensionless wave kinematics ($\Pi_2 = uT/H$), and dimensionless boulder volume ($\Pi_5 = {D_n}^3/H^3$) all made dimensionless using wave height (H). The dimensional analysis applied to this study's experimental data (Fig. 7) includes wave period (within Π_2), to have a greater focus on tsunami waves. Although using two boulders of a similar mass and density in the experiments allowed for enlightening comparisons of the effect of shape, the influence of those parameters is harder to distinguish within Π_6 (Fig. 7). Therefore, these pi groups can be applied to other studies which did not consider shape to further investigate their effectiveness on a wider range of data.

4.2.1. Application of dimensional analysis to other physical experiments and the Settai case study

To obtain a larger dataset for all three dimensionless groups, an experiment conducted by Watanabe et al. (2020) is added to our data and the Settai case study (Fig. 8). The experiment by Watanabe et al. (2020) was chosen for two reasons: 1) all the information needed to calculate the three Π groups was published; 2) the experiment uses a similar set up with a similar boulder starting position, a deep-water

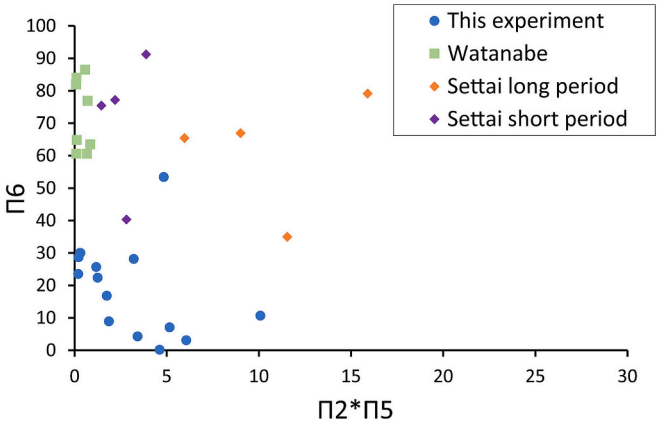


Fig. 8. Pi group graph using mean moved boulder data, with Watanabe et al. (2020) experimental data and Settai field data (Nandasena et al., 2013).

wave flume and a gradually transitioning slope (from 1:10 to 1:100). Other experiments were also considered but owing to their limited number, lack of published wave parameters (Table 1), and differences in wave generation, these were not included in the dimensional analysis.

The experiments conducted by Watanabe et al. (2020) continue the overall laboratory trend but include even greater Π_6 values (Fig. 8). This shows that in laboratory experiments when Π_2*Π_5 is smaller, Π_6 is generally greater. This is caused by both the boulder being smaller (Π_5) and the wave being steeper (a shorter wave period in Π_2). This could be expected because steeper waves are more impulsive. However, laboratory experiments rarely simulate accurate wave periods of tsunami waves; even in this study where waves had long enough periods, large enough wave heights to transport the boulders at a 1:50 scale could not be generated. Extreme wave periods generated by real tsunami waves may have the potential to move boulders farther, owing to the increased duration of the flow (Imamura et al., 2008). Therefore, it is important for future experiments to include as long wave periods as possible with the wave generation method available.

The Settai case study (Fig. 4) provides the opportunity to make connections between physical experiments and real events, whilst also further expanding the data included in the dimensional analysis. Yet the Settai field data (long period) does not fit the overall trend, whereas the short period data is a closer fit (Fig. 8). There are several potential explanations for this discrepancy. The Π_2 group is particularly significant in this case because of the large differences in wave period between the Settai case study (long period) and the scaled-up experimental data (Table 4). At extreme wave periods the transport distance of the boulder could increase, owing to the aforementioned increase in duration of flow, resulting in both large Π_6 and Π_2*Π_5 values. An alternative explanation is that the shorter period, more impulsive waves may be responsible for most of the boulder transport, whilst the longer period waves causing the large inundation have a more limited contribution. This is supported by observations from the experiment, where the longer period waves (e.g., tests # 11–15) had a lower flow velocity ($V < 0.05$ m/s) and so did not transport the boulders despite a significant water travel distance ($X_w = 1.2$–3.3 m). If either of these explanations is the case, it indicates our current tsunami boulder transport experiments may not fully replicate the transport process, and that future experiments should try to replicate both the shorter period and long period wave elements of the 2011 tsunami simultaneously.

Other factors also influence the field data when compared with the experimental data, for example the influence of starting location is known to effect boulder transport. In Settai the boulder source is assumed to have been from subaerial outcrops near the high tide water level (similar to the experiments), but the source could have been partially or fully submerged, which can result in large variance in transport distance. Oetjen et al. (2020) showed that on a rounded boulder model, there is a 40 % increase in transport distance between partially submerged and subaerial starting location. Differences in slope angle between the experiment and the field site could also explain the differences between the Settai and experimental data. In Settai, there is an average slope of approximately 1:100, whereas this experiment was conducted on a steeper 1:30 slope, which would be expected to cause reduced transport distances compared to the field data. However, the Watanabe et al. (2020) experiments also had a 1:100 slope, alongside smaller Π_2*Π_5 values than in Settai, but did not see much greater Π_6 values (Fig. 8). Prior to the tsunami, the Settai river valley was largely occupied by rice fields and light brush. This land use affected the site's roughness, which in turn influenced boulder transport distances. For example, in a valley with a greater surface roughness associated with thick woodland, a lower transport distance would be expected, so roughness is another important parameter to consider in future work.

Real tsunami events also contain sediment, clast and debris interactions, that are not typically represented in the physical experiments (Table 1) which could also influence transport distances (Sugawara et al., 2014). Furthermore, in our experiments we recorded the maximum boulder transport distance, but boulders in the field will experience backwash and may be transported back towards their source (as observed in the experiment) which will also affect recorded transport distances. Although, for the Settai case study specifically most large (>1 m diameter) boulders were unmoved by the backwash because the flow was concentrated in the valley thalweg (Yamada et al., 2014).

To provide further insight into the comparisons of the different experimental and field data, Fig. 9 shows the range of Pi group values for the different datasets. Firstly, Π_2 (uT/H) values for the waves generated in this study offer the widest range of the datasets compared. However, boulders are only transported at much lower Π_2 values than in the Settai long period field example. The Watanabe et al. (2020), this study (moved), and Settai short period data are comparable. This illustrates the discrepancy between the Settai long period data and other datasets, which is largely caused by the difference in wave period. The boulder size relative to wave height, $\Pi_5(D_n^3/H^3)$, has a greater range in this experiment than in the Watanabe et al. (2020) experiments and Settai data, but still overlaps with them particularly for the moved boulders (Fig. 9b). The Watanabe et al. (2020) experiments have large wave heights relative to boulder size causing a low $\Pi_5$value, which when combined with the low $\Pi_2$value offers an interesting extreme of Π_2*$\Pi_5$in Fig. 8.

Values for Π_6 for this experiment are lower than those of the Settai case study, but do have some overlap. Watanabe et al. (2020) shows a much greater overlap with the field case study (Fig. 9c). The similarity in Π_6 between Watanabe et al. (2020) and the Settai case study is likely caused by the more similar beach slope gradient of 1:100 used in the Watanabe et al. (2020) experiments. This is of particular interest because it supports the explanation of gradient being one of the main causes of the Settai long period data plotting differently to the data from this experiment in Fig. 8. Slope was not included as a parameter in this analysis because it was not changed during this study's experiment. However, this highlights that in future work slope should be included to fully complete the dimensional analysis and make accurate comparisons.

Overall, the dimensional analysis allows for comparisons between different physical experiments and field case study examples, and highlights discrepancies in parameters between them. Future work including both physical experiments and field data will build insight into the relationships between offshore wave parameters and boulder transport. These Π groups act as a starting point to explore further ways of comparing field and experimental data, and work towards the goal of hindcasting tsunami waves from transported boulders.

4.3. Implications and future steps

This study highlights several knowledge gaps that need to be overcome to achieve improved techniques for hindcasting tsunami waves using CBDs. The future steps necessary to achieve this include a focus on continued interdisciplinary development. Communication between geomorphologists and researchers conducting physical and numerical investigations to create combined approaches is vital. By approaching the problem from multiple angles with combined datasets a stronger argument can be made for the origins of a real-world CBD, which will have meaningful implications for hazard assessments in coastal regions.

Furthermore, reported field datasets need to be as complete as is feasible. Investigations of recent events should include as much information about the waves that transported the boulders as possible, whether recorded or modelled, to create case study examples for comparison to physical experiments and numerical models. When measuring CBDs, the shape of boulders should be studied beyond their three axes, potentially through photogrammetry (e.g., Boulton and Whitworth, 2018; Nagle-McNaughton and Cox, 2020). The geomorphology of different field sites should additionally be considered. This study focuses on a slightly inclined slope like in a river valley, but other environments

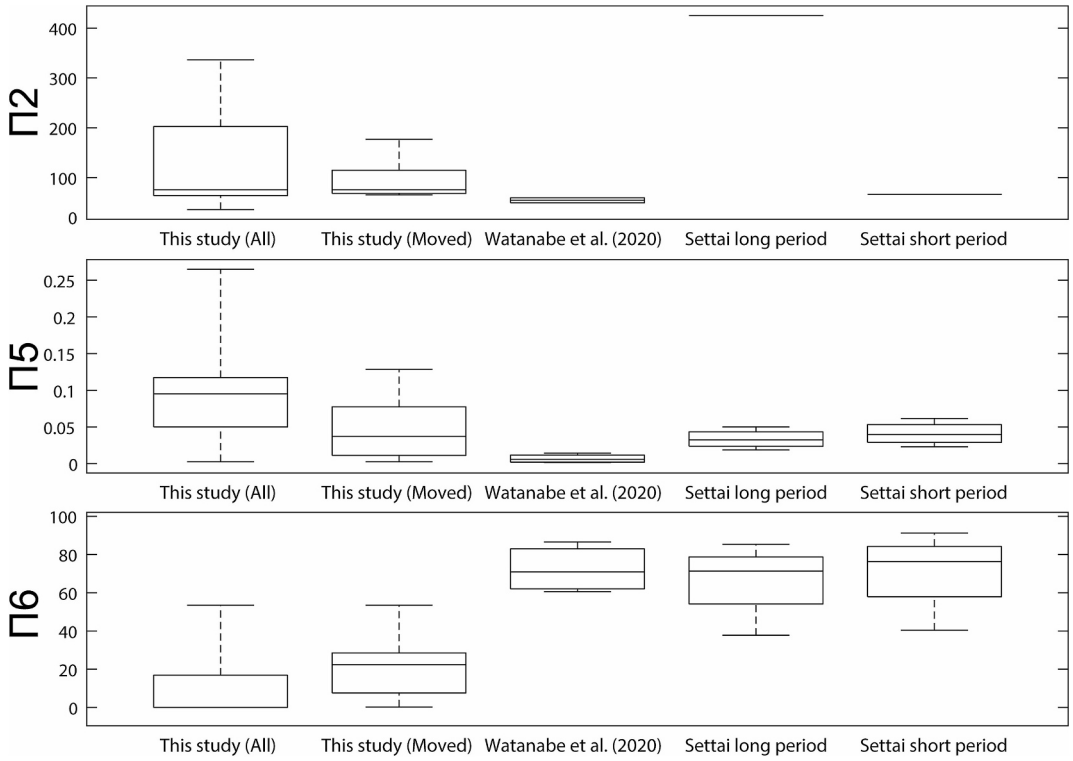


Fig. 9. Pi group comparisons with experimental studies (This study (all); This study (moved boulders only); Watanabe et al., 2020) and Settai long and short period data (Nandasena et al., 2013).

such as boulder beaches and cliff top deposits exist which cannot be directly compared with the same formulation.

Ultimately, more physical experiments are necessary to develop the understanding boulder transport under the influence of tsunami and storm waves. Future physical experiments should aim to measure as many parameters as possible, with a particular focus on flow velocity on the slope, flow depth, offshore wave height and wave period. An array of boulder shapes needs to be studied to understand how shape affects transport distance, allowing for the development of methods to statistically represent the influence of shape on transport. The effect of sediment load and multiple boulders in the flow on boulder transport also requires further investigation. Despite the tsunami simulator's ability to recreate wave properties of the 2011 tsunami in places along the coast of Japan, for Settai it lacks the capability to reach the extremes needed to do so at a 1:50 scale. Therefore, longer wave periods at representative heights are also necessary in future experiments to better represent realistic tsunami events. Similarly, testing the effects of multiple wave tsunami events rather than a solitary wave will also improve our understanding.

The continued development of dimensional analysis to compare studies in the laboratory and field will enable better comparisons to be made, particularly allowing consideration of parameters that could not be included in this study. For example, the shape of the boulder appears to be influential on transport distance, as well as the shore slope. Field and experimental studies can then inform each other, allowing for future interdisciplinary development that can produce a more comprehensive picture.

5. Conclusions

Making connections between CBDs and the causative wave heights is a non-trivial task, which will require the use of novel methods and interdisciplinary study. To build upon previous work, a series of physical experiments were undertaken to investigate the key wave and boulder parameters, with a focus on boulder shape and wave type. The irregular, more rounded and elongate, boulder model generally showed greater transport distances than a cuboid boulder model of a similar mass. Wave type influenced boulder transport distances, with N-waves generally resulting in longer transport distances than E-waves of a similar wave steepness. Further investigation into boulder shape and wave type are necessary, to quantify the influence of a variety of boulder shapes and variable wave parameters on boulder transport distances on different slopes.

Dimensional analysis using Buckingham's Pi Theorem was used to find relationships between key offshore wave and boulder parameters. Connections between a field case study in Settai, where boulders were transported during the 2011 Tohoku tsunami, this experiment, and an experiment by Watanabe et al. (2020) were also investigated using the dimensional analysis. Both the Watanabe et al. (2020) and Settai short period datasets showed a similar trend to this experiment but at greater dimensionless boulder transport values. Interestingly, the Settai long period data did not fit the same trend, possibly because the shorter period, more impulsive waves are linked to boulder motion, whilst the longer periods largely contribute to the horizontal inundation. Although further testing is still needed, with more experimental and field case study examples, to develop a wider dataset and better understand all parameters involved. Future experimental research should also aim to publish all key parameters to enable comparisons like those in this study. Through this additional research dimensionless relationships between parameters such as boulder size, transport distance and offshore wave parameters can be better understood. The dimensional analysis may also be used to inform new approaches attempting to make connections with the offshore wave environment.

Data statement

All data supporting the findings of this study are included within the manuscript and its supplementary materials or are available at https://doi.org/10.24382/d088f83b-f69b-4acc-a704-8eb0e7c7de7f.

CRediT authorship contribution statement

Storm Roberts: Writing – review & editing, Writing – original draft, Project administration, Methodology, Investigation, Formal analysis, Conceptualization. **Alison Raby:** Writing – review & editing, Supervision, Methodology, Investigation, Formal analysis, Conceptualization. **Sarah J. Boulton:** Writing – review & editing, Supervision, Methodology, Formal analysis, Conceptualization. **William Allsop:** Supervision, Methodology, Investigation. **Alessandro Antonini:** Writing – review & editing, Software. **Ivo van Balen:** Investigation. **David Mcgovern:** Writing – review & editing, Software. **Keith Adams:** Investigation. **Ian Chandler:** Software, Resources. **Jonas Cels:** Investigation. **Irene Manzella:** Supervision.

Declaration of competing interest

The authors declare the following financial interests/personal relationships which may be considered as potential competing interests:

Storm Roberts reports financial support was provided by Centre for Doctoral Training (CDT) in Geoscience and the Low Carbon Energy Transition. Alison Raby reports financial support was provided by UK Research and Innovation Natural Environment Research Council. If there are other authors, they declare that they have no known competing financial interests or personal relationships that could have appeared to influence the work reported in this paper.

Acknowledgements

The laboratory experiments presented in this paper are part of the Multidisciplinary Advancement of Knowledge on Extreme Waves (MAKEWAVES) project led by Prof Tiziana Rossetto at UCL. MAKEWAVES has largely been funded by the in-kind contributions of the partner universities and institutions, with HR Wallingford making available the flume facility and providing technical support, UCL contributing monitoring equipment, and Southampton University and TU Delft contributing to consumables. Some grant funding was obtained from the AKT 269 Innovate UK awarded to London South Bank University, and from a Royal Society Exchanges Grant awarded to UCL and TU Delft.

Work was principally conducted by SR, PhD study funded by the Centre for Doctoral Training (CDT) in Geoscience and the Low Carbon Energy Transition, sponsored by the University of Plymouth and Neo-Energy Upstream, whose support is gratefully acknowledged. AR acknowledges funding to visit the Japan field site with SR and SJB, from a NERC "Cross-disciplinary research for Discovery Science" Fellowship Award.

The authors would like to express their gratitude to the editor, Prof Edward Anthony, and the reviewers, including Dr Max Engel and an anonymous reviewer, for their helpful insights and recommendations, which have significantly enhanced the quality of this manuscript.

Appendix A. Supplementary data

Supplementary data to this article can be found online at https://doi.org/10.1016/j.margeo.2024.107474.

References

Barbano, M.S., Pirrotta, C., Gerardi, F., 2010. Large boulders along the south-eastern Ionian coast of Sicily: storm or tsunami deposits? Mar. Geol. 275, 140–154. https://doi.org/10.1016/j.margeo.2010.05.005.

Benner, R., Browne, T., Brückner, H., Kelletat, D., Scheffers, A., 2010. Boulder Transport by Waves: Progress in Physical Modelling. Z. Geomorphol. 54. https://doi.org/10.1127/0372-8854/2010/0054S3-0022. Supplementary Issues.

Boulton, S.J., Whitworth, M.R.Z., 2018. Block and Boulder Accumulations on the Southern Coast of Crete (Greece): Evidence for the 365 CE Tsunami in the Eastern Mediterranean. Geological Society Special Publication. Geol Soc Ldn, pp. 105–125. https://doi.org/10.1144/SP456.4.

Bressan, L., Guerrero, M., Antonini, A., Petruzzelli, V., Archetti, R., Lamberti, A., Tinti, S., 2018. A laboratory experiment on the incipient motion of boulders by high-energy coastal flows. Earth Surf. Process. Landf. 43, 2935–2947. https://doi.org/10.1002/esp.4461.

Buckingham, E., 1915. The Principle of Similitude. Nature 96, 396–397. https://doi.org/10.1038/096396d0.

Chagué-Goff, C., Goff, J., Wong, H.K.Y., Cisternas, M., 2015. Insights from geochemistry and diatoms to characterise a tsunami's deposit and maximum inundation limit. Mar. Geol. 359, 22–34. https://doi.org/10.1016/J.MARGEO.2014.11.009.

Costa, P.J.M., Andrade, C., Freitas, M.C., Oliveira, M.A., da Silva, C.M., Omira, R., Taborda, R., Baptista, M.A., Dawson, A.G., 2011. Boulder deposition during major tsunami events. Earth Surf. Process. Landf. 36, 2054–2068. https://doi.org/10.1002/esp.2228.

Cox, R., Zentner, D.B., Kirchner, B.J., Cook, M.S., 2012. Boulder ridges on the Aran Islands (Ireland): recent movements caused by storm waves, not tsunamis. J. Geol. 120, 249–272. https://doi.org/10.1086/664787.

Cox, R., Jahn, K.L., Watkins, O.G., Cox, P., 2018. Extraordinary boulder transport by storm waves (west of Ireland, winter 2013–2014), and criteria for analysing coastal boulder deposits. Earth Sci. Rev. 177, 623–636. https://doi.org/10.1016/j.earscirev.2017.12.014.

Cox, R., Ardhuin, F., Dias, F., Autret, R., Beisiegel, N., Earlie, C.S., Herterich, J.G., Kennedy, A., Paris, R., Raby, A., Schmitt, P., Weiss, R., 2020. Systematic Review shows that work Done by storm Waves can be Misinterpreted as Tsunami-Related because Commonly used Hydrodynamic Equations are Flawed. Front. Mar. Sci. 7. https://doi.org/10.3389/fmars.2020.00004.

Dawson, A.G., Stewart, I., 2007. Tsunami deposits in the geological record. Sediment. Geol. 200, 166–183. https://doi.org/10.1016/J.SEDGEO.2007.01.002.

Engel, M., May, S.M., 2012. Bonaire's boulder fields revisited: evidence for Holocene tsunami impact on the Leeward Antilles. Quat. Sci. Rev. 54, 126–141. https://doi.org/10.1016/J.QUASCIREV.2011.12.011.

Goto, K., Chavanich, S.A., Imamura, F., Kunthasap, P., Matsui, T., Minoura, K., Sugawara, D., Yanagisawa, H., 2007. Distribution, origin and transport process of boulders deposited by the 2004 Indian Ocean tsunami at Pakarang Cape, Thailand. Sediment. Geol. 202, 821–837. https://doi.org/10.1016/J.SEDGEO.2007.09.004.

Harry, S., Exton, M., Yeh, H., 2019. Boulder Pickup by Tsunami Surge. J Earthq Tsunami 13. https://doi.org/10.1142/S1793431119410069.

Hughes, S.A., 1993. Physical Models and Laboratory Techniques in Coastal Engineering. World Sci. https://doi.org/10.1142/2154.

Imamura, F., Goto, K., Ohkubo, S., 2008. A numerical model for the transport of a boulder by tsunami. J Geophys Res Oceans 113. https://doi.org/10.1029/2007JC004170.

Iwai, S., Goto, K., 2021. Threshold flow depths to move large boulders by the 2011 Tohoku-oki tsunami. Sci. Rep. 11. https://doi.org/10.1038/s41598-021-92917-2.

Kennedy, A.B., Cox, R., Dias, F., 2021. Storm Waves May be the source of some "Tsunami" Coastal Boulder Deposits. Geophys. Res. Lett. 48. https://doi.org/10.1029/2020GL090775.

Landsat, T.M., 2011. Satellite imagery of Settai, Japan, acquired on April 5, 2011. 39°48′45"N 141°58′41"E, elevation 5m. Accessed via Google Earth Pro 7.3.3 on February 12, 2024. https://www.google.com/earth/index.html.

Lau, A.Y.A., Terry, J.P., Switzer, A.D., Pile, J., 2015. Advantages of beachrock slabs for interpreting high-energy wave transport: evidence from ludao island in South-Eastern Taiwan. Geomorphology 228, 263–274. https://doi.org/10.1016/j.geomorph.2014.09.010.

Liu, H., Sakashita, T., Sato, S., 2014. An experimental study on the tsunami boulder movement. ICCE 34.

Lodhi, H.A., Hasan, H., Nandasena, N.A.K., 2020. The role of hydrodynamic impact force in subaerial boulder transport by tsunami—Experimental evidence and revision of boulder transport equation. Sediment. Geol. 408, 105745. https://doi.org/10.1016/J.SEDGEO.2020.105745.

Luccio, P.A., Voropayev, S.I., Fernando, H.J.S., Boyer, D.L., Houston, W.N., 1998. The motion of cobbles in the swash zone on an impermeable slope. Coast. Eng. 33, 41–60. https://doi.org/10.1016/S0378-3839(98)00003-9.

McGovern, D.J., Robinson, T., Chandler, I.D., Allsop, W., Rossetto, T., 2018. Pneumatic long-wave generation of tsunami-length waveforms and their runup. Coast. Eng. 138, 80–97. https://doi.org/10.1016/J.COASTALENG.2018.04.006.

Munson, B.R., Okiishi, T.H., Huebsch, W.W., Rothmayer, A.P., 2014. Fundamentals of Fluid Mechanics. John Wiley & Sons, Inc., Hoboken, NJ, pp. 346–399.

Nagle-McNaughton, T., Cox, R., 2020. Measuring change using quantitative differencing of repeat structure-from-motion photogrammetry: the effect of storms on coastal boulder deposits. Remote Sens. 12, 42. https://doi.org/10.3390/rs12010042.

Nandasena, N.A.K., 2020. Perspective of incipient motion formulas: boulder transport by high-energy waves. Geological Records of Tsunamis and Other Extreme Waves 641–659. https://doi.org/10.1016/B978-0-12-815686-5.00029-8.

Nandasena, N.A.K., Tanaka, N., 2013. Boulder transport by high energy: Numerical model-fitting experimental observations. Ocean Eng. 57, 163–179. https://doi.org/10.1016/J.OCEANENG.2012.09.012.

Nandasena, N.A.K., Paris, R., Tanaka, N., 2011. Reassessment of hydrodynamic equations: Minimum flow velocity to initiate boulder transport by high energy events (storms, tsunamis). Mar. Geol. 281, 70–84. https://doi.org/10.1016/j.margeo.2011.02.005.

Nandasena, N.A.K., Tanaka, N., Sasaki, Y., Osada, M., 2013. Boulder transport by the 2011 Great East Japan tsunami: Comprehensive field observations and whither model predictions? Mar. Geol. 346, 292–309. https://doi.org/10.1016/J.MARGEO.2013.09.015.

Nandasena, N.A.K., Scicchitano, G., Scardino, G., Milella, M., Piscitelli, A., Mastronuzzi, G., 2022. Boulder displacements along rocky coasts: a new

deterministic and theoretical approach to improve incipient motion formulas. Geomorphology 407, 108217. https://doi.org/10.1016/J.GEOMORPH.2022.108217.

Nott, J., 1997. Extremely high-energy wave deposits inside the Great Barrier Reef, Australia: determining the cause—tsunami or tropical cyclone. Mar. Geol. 141, 193–207. https://doi.org/10.1016/S0025-3227(97)00063-7.

Nott, J., 2003. Waves, coastal boulder deposits and the importance of the pre-transport setting. Earth Planet. Sci. Lett. 210, 269–276. https://doi.org/10.1016/S0012-821X(03)00104-3.

Oetjen, J., Engel, M., Pudasaini, S.P., Schuettrumpf, H., 2020. Significance of boulder shape, shoreline configuration and pre-transport setting for the transport of boulders by tsunamis. Earth Surf. Process. Landf. 45, 2118–2133. https://doi.org/10.1002/esp.4870.

Oetjen, J., Engel, M., Schüttrumpf, H., 2021. Experiments on tsunami induced boulder transport – a review. Earth Sci. Rev. https://doi.org/10.1016/j.earscirev.2021.103714.

Open University, 1999. Waves, Tides and Shallow-Water Processes, 2nd ed. Pergamon/Butterworth Heinemann, Oxford. https://doi.org/10.1016/B978-0-08-036372-1.X5000-4.

Pepe, F., Corradino, M., Parrino, N., Besio, G., Presti, V. Lo, Renda, P., Calcagnile, L., Quarta, G., Sulli, A., Antonioli, F., 2018. Boulder coastal deposits at Favignana Island rocky coast (Sicily, Italy): Litho-structural and hydrodynamic control. Geomorphology 303, 191–209. https://doi.org/10.1016/J.GEOMORPH.2017.11.017.

Petroff, C.M., Moore, A.L., Halldor Arnason, H.H., 2001. Particle advection by turbulent bores-Orientation effects Holocene paleoclimate variability in the Tropics View project Particle advection by turbulent bores-Orientation effects. Int Tsunami Symposium 7, 7–23.

Pignatelli, C., Sansò, P., Mastronuzzi, G., 2009. Evaluation of tsunami flooding using geomorphologic evidence. Mar. Geol. 260, 6–18. https://doi.org/10.1016/J.MARGEO.2009.01.002.

Satake, K., Fujii, Y., Harada, T., Namegaya, Y., 2013. Time and space distribution of coseismic slip of the 2011 Tohoku earthquake as inferred from Tsunami waveform data. B Seismol Soc AM 103 (2 B), 1473–1492. https://doi.org/10.1785/0120120122.

Shah-hosseini, M., Morhange, C., Naderi Beni, A., Marriner, N., Lahijani, H., Hamzeh, M., Sabatier, F., 2011. Coastal boulders as evidence for high-energy waves on the Iranian coast of Makran. Mar. Geol. 290, 17–28. https://doi.org/10.1016/j.margeo.2011.10.003.

Shimozono, T., Cui, H., Pietrzak, J.D., Fritz, H.M., Okayasu, A., Hooper, A.J., 2014. Short Wave Amplification and Extreme Runup by the 2011 Tohoku Tsunami. Pure Appl. Geophys. 171, 3217–3228. https://doi.org/10.1007/s00024-014-0803-1.

Sugawara, D., Goto, K., Jaffe, B.E., 2014. Numerical models of tsunami sediment transport — current understanding and future directions. Mar. Geol. 352, 295–320. https://doi.org/10.1016/J.MARGEO.2014.02.007.

Svendsen, I.A., 2006. Introduction to Nearshore Hydrodynamics. WORLD SCIENTIFIC. https://doi.org/10.1142/5740.

Watanabe, M., Yoshii, T., Roeber, V., Goto, K., Imamura, F., 2020. Data of boulder transport experiment in super-large wave flume. J Sediment Soc Jpn 79, 15–25.

Williams, D.M., Hall, A.M., 2004. Cliff-top megaclast deposits of Ireland, a record of extreme waves in the North Atlantic—storms or tsunamis? Mar. Geol. 206, 101–117. https://doi.org/10.1016/J.MARGEO.2004.02.002.

Yamada, M., Fujino, S., Goto, K., 2014. Deposition of sediments of diverse sizes by the 2011 Tohoku-oki tsunami at Miyako City, Japan. Mar. Geol. 358, 67–78. https://doi.org/10.1016/J.MARGEO.2014.05.019.

Yamazaki, Y., Cheung, K.F., Lay, T., 2018. A Self-Consistent Fault Slip Model for the 2011 Tohoku Earthquake and Tsunami. J. Geophys. Res.: Solid. Earth 123 (2), 1435–1458. https://doi.org/10.1002/2017JB014749.

Yang, S., Yang, W., Zhang, C., Qin, S., Wei, K., Zhang, J., 2022. Experimental and numerical study on the evolution of wave front profile of dam-break waves. Ocean Eng. 247, 110681. https://doi.org/10.1016/j.oceaneng.2022.110681.